CARMA: A ROBUST MOTION ARTIFACT REDUCTION ALGORITHM FOR HEART RATE MONITORING FROM PPG SIGNALS

Alessandro Bacà, Giorgio Biagetti, Marta Camilletti, Paolo Crippa, Laura Falaschetti,
Simone Orcioni, Luca Rossini, Dario Tonelli, Claudio Turchetti

DII – Dipartimento di Ingegneria dell'Informazione, Università Politecnica delle Marche
Via Brecce Bianche 12, I-60131 Ancona, Italy
e-mail: c.turchetti@univpm.it

ABSTRACT

Photoplethysmography (PPG) is a non invasive measurement of the blood flow, that can be used instead of electrocardiography to estimate heart rate (HR). Most existing techniques used for HR monitoring in fitness with PPG focus on slowly running alone, while those suitable for intensive physical exercise need an initialization stage in which wearers are required to stand still for several seconds. This paper present a novel algorithm for HR estimation from PPG signal based on motion artifact removal (MAR) and adaptive tracking (AT) that overcomes limitations of the previous techniques. Experimental evaluations performed on datasets recorded from several subjects during running show an average absolute error of HR estimation of 2.26 beats per minute, demonstrating the validity of the presented technique to monitor HR using wearable devices which use PPG signals.

Index Terms— Heart rate monitoring, photoplethysmography (PPG), motion artifact, SVD decomposition.

1. INTRODUCTION

Photoplethysmography (PPG) is a non invasive measurement of the blood flow at the surface of the skin, that is used instead of electrocardiography (ECG) to estimate heart rate (HR).

In new wearable devices this signal needs to be monitored during fitness and/or daily activities where motion is always present. HR monitoring from wrist type PPG signal during intensive physical exercise is a challenging problem due to the extremely strong motion artifact (MA), caused by subjects' hand movements, that corrupts PPG signal.

To date, several different techniques have been suggested for the removal of MA from PPG signal. Among these, the most common are: independent component analysis (ICA) [1], adaptive filtering techniques [2, 3], Kalman filtering [4], wavelet based methods [5], empirical mode decomposition [6, 7]. More recently combinations of a number of techniques have been successful used [8, 9]. The main lacks of these are as follows. Most of them were proposed for a clinical scenario, that is with subjects performing small motions. Only a few techniques are suitable for HR monitoring in fitness. However, some of them focused on slowly running alone, while techniques for intensive physical exercise need an initialization stage in which wearers are required to reduce hand motions as much as possible for several seconds.

The algorithm presented in this paper aims to overcome all the limitations of the previous techniques. The algorithm consists of two key parts: motion artifact removal (MAR) and adaptive tracking (AT).

The MAR algorithm is based on the assumption that the artifact and heart rate signal are in two distinct subspaces. The subspace of motion signals (SMS) is estimated by the singular value decomposition (SVD) of the accelerometer data matrix, while the subspace of the HR signal is estimated by removing the closest subspace to the SMS from the SVD decomposition of the PPG data matrix.

The AT algorithm is based on the assumption that each of the main components extracted by the SVD show a single dominant peak in their frequency spectrum. We determine the frequency of these peaks and use them to define a metric to measure distances between the SMS and potential HR estimates, so that MAs can be removed. Then the sequence of HR estimates so obtained is smoothed to prevent spurious residual artifacts from affecting the result. One strong point of the employed adaptive smoothing algorithm is that it is able to converge to the true HR track regardless of the starting point, thus relieving the subject from the need of limiting their motion to initialize the PPG tracking.

2. MATHEMATICAL FRAMEWORK

A flow chart of the overall algorithm, named Closest-subspace Algorithm for Reducing Motion Artifact (CARMA), is shown in Fig. 1. It consists of the following main steps: *i)* pre-processing (windowing, filtering and Hankel data matrix construction) of PPG and accelerometer signals, *ii)* SVD decomposition, *iii)* peak detection of the FFTs, *iv)* motion artifact reduction, *v)* tracking of the heart rate. Steps *i)–iii)* are used to determine the SMS, steps *iv)–v)* perform the AT, as detailed next.
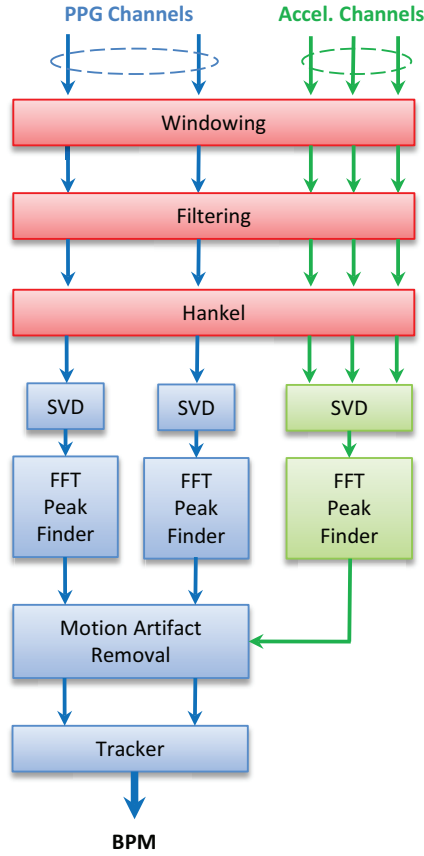
Fig. 1: Flow chart of CARMA algorithm.

2.1. Subspace of motion signals

Given the accelerometer signals x, y, z the first step is to determine the corresponding subspace $\langle S \rangle$ they belong to, that is a basis S that generates $\langle S \rangle$. To this end let $X = \left[x^{(1)} \ldots x^{(L)} \right]$, $Y = \left[y^{(1)} \ldots y^{(L)} \right]$, $Z = \left[z^{(1)} \ldots z^{(L)} \right]$ be the Hankel data matrices of the three signals respectively, where $x^{(i)}, y^{(i)}, z^{(i)} \in \mathbb{R}^N$, $i = 1, \ldots, L$, $L > N$ represent the observations achieved from the three-axes accelerometer.

The complete matrix of sample signals

$$H = [X \, Y \, Z] \in \mathbb{R}^{N \times 3L} \qquad (1)$$

can be decomposed by the SVD as

$$H = \tilde{S} \Lambda R^T = \sum_{i=1}^{N} \lambda_i s_i r_i^T, \qquad (2)$$

where $\tilde{S} = [s_1 \ldots s_N]$, $R = [r_1 \ldots r_N]$ and the eigenvalues λ_i are in decreasing order $\lambda_1 \geq \lambda_2 \geq \ldots \geq \lambda_N$. Since, in general, it results $\lambda_{P+1}, \ldots, \lambda_N < \varepsilon$ with $\varepsilon \approx 0$ we can write

$$H \cong \sum_{i=1}^{P} \lambda_i s_i r_i^T. \qquad (3)$$

This approximation is equivalent to assume the signals are in the subspace

$$\langle S \rangle = \text{span}\,(s_1 \ldots s_P) \,, \qquad (4)$$

generated by the basis $S = [s_1 \ldots s_P] \in \mathbb{R}^{N \times P}$ where $s_1 \ldots s_P$ are the most significative components of the motion signal. $\langle S \rangle$ represents the SMS.

2.2. PPG signal model

Let us assume the following model for the PPG signal

$$g = m + e \quad, \qquad g \in \mathbb{R}^N \qquad (5)$$

where e is the heart-rate signal, m the artifact and g the PPG signal. As m belongs to the subspace $\langle S \rangle$, then the corresponding Hankel data matrix $G = \left[g^{(1)} \ldots g^{(L)} \right]$, $G \in \mathbb{R}^{N \times L}$ can be written as

$$G = SA + E \qquad (6)$$

with $A = \left[a^{(1)} \ldots a^{(L)} \right] \in \mathbb{R}^{P \times L}$, $E = \left[e^{(1)} \ldots e^{(L)} \right] \in \mathbb{R}^{N \times L}$.

It is worth to note that, as $\tilde{S}$ can be decomposed in two orthonormal subsets $S, S_\perp$

$$\tilde{S} = [s_1, \ldots, s_P, s_{P+1}, \ldots s_N] = [S \, S_\perp] \qquad (7)$$

with $S_\perp = [s_{P+1}, \ldots s_N]$, E decomposes into two components, belonging to the two orthogonal subspaces $\langle S \rangle, \langle S_\perp \rangle$

$$E = [S \, S_\perp] \begin{bmatrix} B \\ B_\perp \end{bmatrix} = SB + S_\perp B_\perp \qquad (8)$$

where $B, B_\perp$ are the corresponding coordinates, so that G is given by

$$G = SA + SB + S_\perp B_\perp = S(A + B) + S_\perp B_\perp \,. \qquad (9)$$

Assuming the component SB of E belonging to the subspace $\langle S \rangle$ is negligible when comparing with the artifact component SA we have

$$G = SA + E \simeq SA + S_\perp B_\perp \,, \qquad (10)$$

and

$$E \simeq S_\perp B_\perp \,. \qquad (11)$$

(10) shows that the artifact and the heart-rate signal belong to two orthonormal subspaces $S, S_\perp$.

2.3. Removing the closest subspace to $\langle S \rangle$ from SVD decomposition of G

It is well known that the SVD decomposes the given space $\mathbb{R}^N$ in orthonormal subspaces. To this end let

$$G = U \Sigma V^T \qquad (12)$$

be the SVD of G, where $U = [u_1 \ldots u_N] \in \mathbb{R}^{N \times N}$, $V = [v_1 \ldots v_L] \in \mathbb{R}^{L \times L}$, and $\Sigma \in \mathbb{R}^{N \times L}$.

This is useful to derive the two components SA, E by selecting vectors u_i belonging to the subspace $\langle S \rangle$. Indeed, assuming $u_i \in R^N$ belongs to the span of S, is equivalent to require that the following equations

$$u_i = S h_i \qquad (13)$$

with unknown constants $h_i \in \mathbb{R}^P$ are satisfied. However, since such a system of equations is not invertible, we search for the vectors u_i that are the closest to the subspace $\langle S \rangle$.

To do this we proceed as follows.

First the spectral peaks of the vectors s_i, u_i are derived. Formally we compute the vectors of frequencies $(k_1(s_1), \ldots, k_P(s_P))$, $(k'_1(u_1), \ldots, k'_N(u_N))$, as given by

$$k_j = \operatorname*{argmax}_k \mathrm{FT}(s_j)(k) \quad , \qquad j = 1, \ldots, P \,, \qquad (14)$$

$$k'_i = \operatorname*{argmax}_k \mathrm{FT}(u_i)(k) \quad , \qquad i = 1, \ldots, N \,, \qquad (15)$$

where FT denotes the Fourier transform. Then we define the distance of the generic vector u_i to the subspace $\langle S \rangle$ as

$$d_i = \min_j |k'_i(u_i) - k_j(s_j)| \quad , \qquad i = 1, \ldots, N \,. \qquad (16)$$

Finally the vectors $(u_{i_1} \ldots u_{i_Q})$ are chosen such that the corresponding distances are below a given threshold ϑ. This mean that the subspace $\langle U_q \rangle = \operatorname{span}(u_{i_1} \ldots u_{i_Q})$ is the closest to the artifact subspace $\langle S \rangle$.

Let Q be the number of such chosen vectors, while we call $i_{Q+1}, \ldots, i_N$ the indices of the remaining vectors (those with distances above the threshold), ordered such that $i_{Q+1} < i_{Q+2} < \cdots < i_N$ so as to maintain the decreasing ordering of the corresponding singular values.

Then consider the following decomposition with $q = [i_1 \ldots i_Q]$, $d = [i_{Q+1} \ldots i_N]$, so that $U_q = [u_{i_1} \ldots u_{i_Q}] \in \mathbb{R}^{N \times Q}$, $U_d = [u_{i_{Q+1}} \ldots u_{i_N}] \in \mathbb{R}^{N \times (N-Q)}$, and so on. It results

$$G = [U_q\,U_d] \begin{bmatrix} \Sigma_q & 0 \\ 0 & \Sigma_d \end{bmatrix} \begin{bmatrix} V_q^T \\ V_d^T \end{bmatrix} = U_q \Sigma_q V_q^T + U_d \Sigma_d V_d^T \,. \qquad (17)$$

Assuming the vectors $(u_{i_1} \ldots u_{i_Q})$ belong to the subspace $\langle S \rangle$ and posing

$$\Sigma_q V_q^T = \begin{bmatrix} b^{(1)} \ldots b^{(L)} \end{bmatrix} \qquad (18)$$

it follows that every column of the matrix

$$U_q \Sigma_q V_q^T = \begin{bmatrix} U_q b^{(1)} \ldots U_q b^{(L)} \end{bmatrix} \qquad (19)$$

belong to $\langle S \rangle$. Comparing (10) with (17) we finally have

$$\begin{cases} SA \simeq U_q \Sigma_q V_q^T \\ E \simeq U_d \Sigma_d V_d^T \end{cases} . \qquad (20)$$

2.4. Tracking

Thanks to the geometrical separation previously performed, the spectrum of the signal so obtained clearly shows the cardiac frequency of the heart-rate signal. In particular, the heart rate can almost always be found as the dominant frequency of the first column of U_d, i.e., as $k'_{i_{Q+1}}$.

However, although usually very good, the artifact removal performed as stated before is not always perfect. To reduce the heart rate estimation error a frequency tracking algorithm is thus necessary. The tracking also tries to combine the signals from the two available PPG channels, as follows.

First a check is made to determine if, by chance (e.g., because the fundamental frequency overlaps a motion artifact), the extracted frequency is a harmonic of the heart rate, and it is halved or doubled according to the result being more likely to be a plausible estimate. This is done exploiting a rough estimate of the joint probability density function of the heart rate versus the motion artifact frequency (MAF). Indeed, it is easy to see from the training data that HR and MAF are positively correlated with a correlation coefficient of about 0.57. This is not a very strong correlation but it is usually enough to tell the fundamental and its harmonics apart, using the likelihood computed over a simple single Gaussian model of the HR, MAF statistics.

Then, to select the best of the two PPG channels, the one that is closest to the previous estimate is chosen. Let d_0 be this distance and e_{t-1} be the previous heart rate estimate. The current estimate e_t is found by tracking the frequency $f_t = k'_{i_{Q+1}}(t)$ of the selected peak, i.e.

$$e_t = k\,e_{t-1} + (1-k)\,f_t \qquad (21)$$

where $k \in [0,1]$ is a weighing factor that increases as the distance of f_t from e_{t-1} increases. As higher k means we rely more on the previous estimates, while lower k means we trust more the current estimate, this parameter can be adjusted to filter out spurious estimates while simultaneously tracking relatively rapid heart rate variations. In our experiments we got good results with a simple piecewise linear model for k as a function of d_0,

$$k = k_{\min} + (k_{\max} - k_{\min})\,\min\{1, d_0/d_\infty\} \qquad (22)$$

where $k_{\min} = 0.1$, $k_{\max} = 0.9$, and $d_\infty = 14\,\mathrm{BPM}$.

Setting a $k_{\min} > 0$ makes the tracking algorithm robust with respect to the tracking starting point, or a few missed estimations, as a sufficiently high number of correct HR estimates will eventually attract the tracking algorithm to the correct path. This is shown experimentally in Fig. 2, which reports the tracking performed from arbitrarily chosen starting points of 30 BPM, 60 BPM, 180 BPM, and 240 BPM (red lines), together with the automatically selected starting point (green line). As a reference, the true HR (derived from simultaneously recorded ECG) is also reported in black. After a few seconds, all the estimated tracks converge to the same, which is also very close to the true HR.
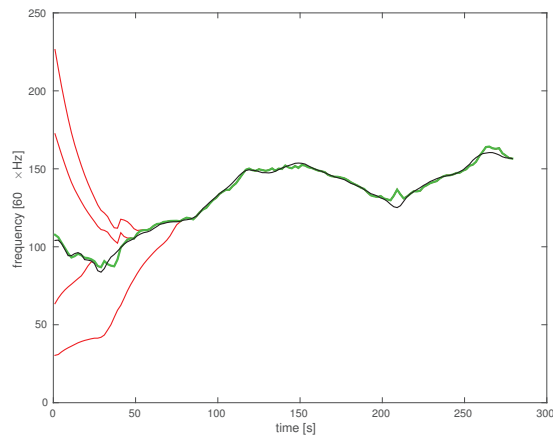
Fig. 2: AT algorithm at work with different starting points (red lines). Regardless of initialization, it always converges to the same track (green line), which is very close to the ground truth (black line).

3. EXPERIMENTAL RESULTS

To validate the effectiveness of the algorithm we tested it on the 12-subject dataset used in [9], and on an extra track (subject 13) in which the subject did a different kind of exercise. Figure 3 shows examples of the tracking performed. The red and amber stars represent the frequency estimates coming from the peak finders for the two PPG channels. The blue circles the frequency estimate of the most prominent peak in the accelerometer channels (actually, $P = 10$ peaks are used in the artifact removal, but only the first is shown to avoid cluttering the figures). The green solid line is our HR estimate. As a reference, the ECG-derived true HR is the black solid line. The tracking is generally good, and even if the algorithm is sometimes driven off the correct track (because the MAR algorithm was overly aggressive and removed a valid HR candidate, or the MA frequency lay so close to the HR that the SVD frequency resolution couldn't resolve them), it soon recovers.

A comparison of its performance with those of [9] are reported in Tab. 1, which reports the mean absolute error (MAE) and the root mean square error (RMSE), and in more detail for each subject in Tab. 2. Despite being much simpler and not requiring an initialization phase, our algorithm attained comparable scores, often remarkably better.

4. CONCLUSIONS

A novel algorithm for HR estimation from PPG signals has been presented. It removes motion artifacts and adaptively tracks HR exploiting dominant frequencies of SVD decomposition to separate the PPG in two subspaces, overcoming many limitations of already existing techniques. Experimental evaluations performed on datasets recorded from subjects

Table 1: Average performance on recordings 1–12 [BPM].

Method	MAE	RMSE
CARMA	2.26	3.63
TROIKA	2.34	3.07

during running and other activities show an average absolute error better than the current state of the art, despite the proposed algorithm being much simpler.

REFERENCES

[1] B. S. Kim and S. K. Yoo, "Motion artifact reduction in photoplethysmography using independent component analysis," *IEEE Trans. Biomedical Engineering*, vol. 53, no. 3, pp. 566–568, March 2006.

[2] J. Y. A. Foo, "Comparison of wavelet transformation and adaptive filtering in restoring artefact-induced time-related measurement," *Biomedical Signal Processing and Control*, vol. 1, no. 1, pp. 93–98, 2006.

[3] P. T. Gibbs, L. B. Wood, and H. H. Asada, "Active motion artifact cancellation for wearable health monitoring sensors using collocated MEMS accelerometers," in *Smart Structures and Materials*. International Society for Optics and Photonics, 2005, vol. 5765, pp. 811–819.

[4] B. Lee *et al.*, "Improved elimination of motion artifacts from a photoplethysmographic signal using a Kalman smoother with simultaneous accelerometry," *Physiological Measurement*, vol. 31, no. 12, pp. 1585, 2010.

[5] M. Raghuram, K. V. Madhav, E. H. Krishna, and K. A. Reddy, "Evaluation of wavelets for reduction of motion artifacts in photoplethysmographic signals," in *10th Int. Conf. Information Sciences Signal Processing and their Applications (ISSPA)*, May 2010, pp. 460–463.

[6] M. Raghuram, K. Sivani, and K. A. Reddy, "E2MD for reduction of motion artifacts from photoplethysmographic signals," in *Int. Conf. Electronics and Communication Systems (ICECS)*, Feb 2014, pp. 1–6.

[7] M. Raghuram *et al.*, "HHT based signal decomposition for reduction of motion artifacts in photoplethysmographic signals," in *IEEE Int. Instrum. Meas. Tech. Conf. (I2MTC)*, May 2012, pp. 1730–1734.

[8] M. R. Ram *et al.*, "A novel approach for motion artifact reduction in PPG signals based on AS-LMS adaptive filter," *IEEE Trans. Instrum. Meas.*, vol. 61, no. 5, pp. 1445–1457, May 2012.

[9] Z. Zhang, Z. Pi, and B. Liu, "TROIKA: A general framework for heart rate monitoring using wrist-type photoplethysmographic signals during intensive physical exercise," *IEEE Trans. Biomedical Engineering*, vol. 62, no. 2, pp. 522–531, Feb 2015.

Table 2: Average absolute error on 12 recordings [BPM].

Method	Subj1	Subj2	Subj3	Subj4	Subj5	Subj6	Subj7	Subj8	Subj9	Subj10	Subj11	Subj12
CARMA	2.58	1.48	1.40	2.47	1.54	3.24	1.01	1.19	0.93	6.28	1.68	3.30
TROIKA	2.29	2.19	2.00	2.15	2.01	2.76	1.67	1.93	1.86	4.70	1.72	2.84

Fig. 3: Experimental results from six different subjects.